# Magnetic effect on the interfacial energy of the Ni(111)/Cr(110) interface

**Song Lu[1], Hualei Zhang[2], Qing-Miao Hu[3], Marko P. J. Punkkinen[4], Börje Johansson[1,5] and Levente Vitos[1,5,6]**

[1]Applied Materials Physics, Department of Materials Science and Engineering, Royal Institute of Technology, Stockholm SE-100 44, Sweden
[2]Center of Microstructure Science, Frontier Institute of Science and Technology, Xi'an Jiaotong University, Xi'an, 710054, China
[3]Shenyang National Laboratory for Materials Science, Institute of Metal Research, Chinese Academy of Sciences, 72 Wenhua Road, Shenyang 110016, China
[4]Department of Physics and Astronomy, University of Turku, FI-20014 Turku, Finland
[5]Department of Physics and Astronomy, Division of Materials Theory, Uppsala University, Box 516, SE-751210, Uppsala, Sweden
[6]Wigner Research Centre for Physics, Institute for Solid State Physics and Optics, H-1525 Budapest, P.O. Box 49, Hungary

**Abstract.** Work of separation and interfacial energy of Ni(111)/Cr(110) interface are calculated via first-principles methods. Both coherent and semicoherent interfaces are considered. We find that magnetism has significant effect on the interfacial energy, i.e., removing magnetism decreases the interfacial energy of semicoherent interface by around 50%. Electronic, magnetic and atomic structures at the interface are discussed. An averaging scheme is used to estimate the work of separation and interfacial energy of semicoherent interfaces based on the results of coherent interfaces. The limitations of the scheme are discussed.

## 1. Introduction

Heterophase interfaces between face-centered-cubic (fcc) and body-centered-cubic (bcc) phases exist in many important alloys, such as Fe-Cu, Fe-Ni, Fe-Ag, Ni-Cr, Cu-Cr or duplex stainless steels. The interfacial properties are very important, for example, when studying the precipitate growth kinetics and interface strengthening or failure mechanisms. It has been shown that the interfacial energy is a key parameter determining the nucleation barrier and also the shapes of precipitates. [1–3] For example, Tóth et al.[4] showed that a reasonable prediction of the fcc-bcc phase boundary in the Fe-Ni system relies on the realistic choice of the fcc/bcc interfacial energy. Unfortunately, the interfacial energy is most often not accessible. Due to the lack of measured data, ab initio calculations have been extensively applied to determine the metal-ceramic interfacial energy. [5] However, for the metallic fcc/bcc interface theoretical studies are very limited.

Ni-Cr is an extensively studied system with fcc/bcc interphase boundaries. Detailed studies of the interfacial structures of bcc precipitates and the kinetics of growth ledge formation have been reported in many publications.[6–10] In Ni-Cr

alloys, the bcc precipitates in lath shape prefer to adopt the Kurdjumov-Sachs (K-S) orientation relationship (OR) and their habit plane lies close to the $(1\bar{2}1)_{\rm fcc}$ with some deviations from one precipitate to another. [6–9, 11] The deviations from the exact $\{111\}_{\rm fcc}\|\{110\}_{\rm bcc}$ and $<110>_{\rm fcc}\|<111>_{\rm bcc}$ are less than 6°. [10] The broad interface between bcc precipitate and fcc matrix is semicoherent with misfit compensating defects, such as structure ledges and irregularly spaced dislocations. [8] By introducing the structure ledges, the interfacial coherency can be significantly increased. [12, 13] Structure ledges are composed of the $(1\bar{1}1)_{\rm fcc}$ and $(0\bar{2}0)_{\rm fcc}$ facets. [14] Despite of extensive studies on the interface structures (e.g., orientation relationships, habit plane, misfit dislocations and structure ledges, etc.), quantitative determination of the interfacial energy is rare. Many studies were suffered from the lack of the interfacial energy. [2, 9, 10] Experimentally, the only effort was made by Hoptkins et al.[11] who estimated the interfacial energy of the eutectic interface in Ni-51 at.% Cr alloys from solidification data to be about 0.30 J $m^{-2}$. This interface was formed between the $\gamma$-Ni-rich and the $\alpha$-Cr-rich phases. On the theoretical side, the embedded atom method (EAM) was adopted by Chen et al. [14] to estimate the fcc/bcc interfacial energy in Ni-Cr alloys. That interface was between fcc Ni-Cr solid solution and bcc Cr. The EAM interfacial energy varies from ∼0.22 J $m^{-2}$ for the pure Ni fcc phase to 0.20 J $m^{-2}$ for the Ni-50 at.% Cr one. These authors concluded that the composition dependence of interfacial energy is weak. By comparing to the EAM fcc-Fe/bcc-Fe interfacial energy (∼0.18 J $m^{-2}$) which has only structure contribution, [8] they further claimed that the main contribution to the Ni/Cr interfacial energy is from the structure difference. However, the energies provided by EAM usually have limited applicability. For example, from the Mayer-Entel type of EAM potential the interfacial energies of fcc-Fe/bcc-Fe interfaces were estimated to be 3.84 J $m^{-2}$ for the Nishiyama-Wasserman (N-W) OR and 2.88 J $m^{-2}$ for the K-S OR. Note that these energies include the contribution from interface dislocation core, without which the interfacial energy for the N-W OR decreases to 0.96 J $m^{-2}$. [15] The interfacial energy of the fcc-Fe/bcc-Fe calculated by Yang and Johnson using an ad-hoc constructed interatomic interaction potential is between 0.24 J $m^{-2}$ and 0.46 J $m^{-2}$, depending on the structure of the interface. [16]

In the present work, we use methods based on the density functional theory (DFT) [17] to study the interface between fcc-Ni and bcc-Cr. Experimental work has shown that during nucleation and in the early stage of growth, precipitates usually match the matrix coherently, which minimizes the interfacial energy. [18] They may lose coherency during continued growth when the elastic strain energy contribution to the total free energy of the system becomes dominant. Formation of misfit dislocations within the interface relieves misfit stress at the expense of increasing interfacial energy. [2]

The coherent interface can be accurately studied by using DFT calculations, however, without considering the lattice mismatch or lattice relaxation. [19, 20] A good and consistent agreement in the description of the coherent interfaces (e.g., work of separation and interfacial energy) using the EAM potentials and DFT calculations would add more reliability for further applications of the EAM potentials to semicoherent or incoherent interfaces. [21, 22] However, to model a realistic semicoherent interface composed of structure ledges, misfit dislocations and coherent patches requires very large supercells which are normally beyond the capacities of nowadays DFT methods. Compromise has to be made. In the present work, we chose a relatively large supercell to decrease the lattice mismatches at the interface, however,

without explicitly including dislocations or structure ledges. [5] In the following, such arrangement is called "semicoherent" interface. When the supercell is properly chosen, it may represent a large fraction of the real semicoherent interface. Two basic energetic variables, work of separation ($W$) and interfacial energy ($\gamma$), are calculated for both coherent and semicoherent interfaces. An effort is made to estimate the work of separation and interfacial energy of the semicoherent interface using the coherent results based on the previously established averaging scheme. [20]

The rest of this paper is arranged as follows: we describe the interface models and the calculation details in Section 2. The results for coherent and semicoherent interfaces together with discussions are presented in Section 3.1 and 3.2. Discussion about the averaging scheme is presented in Section 3.3. Finally, the summary is presented in Section 4.

## 2. Methodology and computational details

### *2.1. Density functional theory method*

The density functional theory [17] calculations are performed by using the Vienna ab initio simulation package (VASP) [23–25] employing the Perdew-Burke-Ernzerhof (PBE) [26] generalized gradient approximation (GGA) for the exchange and correlation energy. The projector augmented-wave (PAW) [27] method is applied. For both bulk and interface calculations the cutoff energies are set to 400 eV for both Ni and Cr. For the bulk calculations, a Monkhorst-Pack mesh of $21 \times 21 \times 21$ k points is employed to sample the Brillouin zone. However, the Gamma-centered grids of $11 \times 13 \times 1$ are adopted for the coherent interfaces and the surface calculations. A k-mesh of $2 \times 4 \times 2$ is used for the calculations of the semicoherent interface. The models of coherent and semicohernet interfaces are described in the following sections. When atomic relaxations are allowed, the forces on atoms are converged to less than 0.02 eV/Å.

### *2.2. Coherent interface*

The crystalline structure of Cr is approximated as antiferromagnetic B2 below its Néel temperature (308K). Nickel is ferromagnetic having the fcc structure. The lattice parameters of Ni and Cr are calculated to be 3.52 Å and 2.86 Å, respectively, which agree well with the experimental values, 3.52 Å for Ni and 2.88 Å for Cr. [28] The calculated magnetic moments are 0.62 $\mu_{\mathrm{B}}$ for Ni and 1.07 $\mu_{\mathrm{B}}$ for Cr.

The smallest misfit ($\delta$) between two lattices is calculated by,

$$\delta = 2\frac{d_{\mathrm{fcc}}^{(111)} - d_{\mathrm{bcc}}^{(110)}}{d_{\mathrm{fcc}}^{(111)} + d_{\mathrm{bcc}}^{(110)}} = 0.41\%, \tag{1}$$

where $d_{\mathrm{fcc}}^{(111)}$ and $d_{\mathrm{bcc}}^{(110)}$ are the plane spacings of fcc(111) and bcc(110), respectively. Experimental study showed that the mismatch between the interlayer spacings of Ni(111) and Cr(110) is accommodated by elastic strain. [8] However, to form coherency between the Ni(111) and Cr(110) facets requires much larger in-plane misfit strains realized by distorting Cr lattice or/and Ni lattice. Larger strains are usually expected to occur for the softer material. In the present work, to make our results/discussion more general for fcc/bcc type of interface, we consider two extreme cases. Case I corresponds to distorting Ni to match equilibrium Cr and case II to distorting Cr to match equilibrium Ni, see Fig. 1. For case I, the coherent interface takes bcc Cr

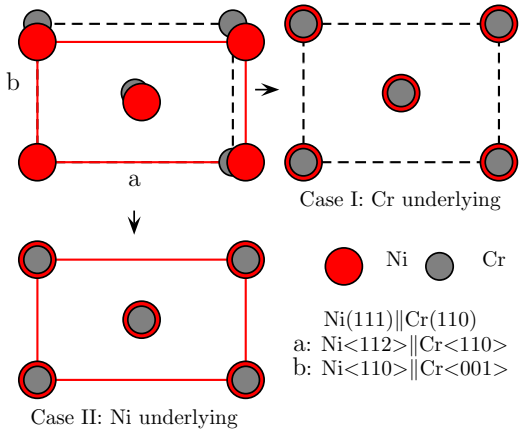


Figure 1: (Color online) Schematic of the coherent Ni(111)/Cr(110) interfaces.

as the underlying lattice and has two atoms per layer, with lateral lattice constants a=4.04Å and b=2.86 Å. The conjugated interface planes are Ni(111) paralleling with Cr(110). In this case, Ni lattice is distorted by +15.02% (elongated) along the <110> and by -6.08% (compressed) along the <112> directions. We test the convergence with respect to the number of layers and use a supercell containing 7 layers of Cr(110) and 7 layers of Ni(111) plus a vacuum layer which is about 20 Å. The two Cr atoms in the same layer are antiferromagnetic coupled, while Ni atoms are ferromagnetic. Atomic relaxation along the direction perpendicular to the interface is preformed.

For case II, taking Ni as the underlying lattice, coherency is obtained by stretching Cr by 6.45% along Cr<110> and by compressing about 13.08% along Cr<001>. Under such strains, we find that the magnetic moments of both bulk and surface Cr atoms drop to around 0 $\mu_{\mathrm{B}}$.

### *2.3. Work of separation and interfacial energy*

The work of separation ($W$) is defined as the energy required per unit area to reversibly separate a bulk material into two semi-infinite bulks with two free surfaces. It is sometimes also named as the "ideal work of separation". [19, 29] In the present study, $W$ is calculated according to

$$W = [E_{\mathrm{Ni}} + E_{\mathrm{Cr}} - E_{\mathrm{Ni/Cr}}]/A, \tag{2}$$

where $E_{\mathrm{Ni}}$ and $E_{\mathrm{Cr}}$ are the total energies of the Ni and Cr slabs with free surfaces, respectively, $E_{\mathrm{Ni/Cr}}$ is the total energy of the Ni/Cr supercell slab embedded in vacuum and $A$ is the area of the interface. All systems were calculated under exactly the same conditions (k-mesh, cutoff energy, etc.). They were all subject to the same lateral lattice strain set by the underlying lattice. Perpendicular to the interface, all the atoms were fully relaxed. The work of separation calculated in this manner gives direct information regarding the strength and bonding of the interface, [29] and was taken as a measure for the mechanical stability and chemical bonding at the interface. [30]

The interfacial energy $\gamma$ is calculated as

$$\gamma = (E^{*}_{\mathrm{Ni/Cr}} - E^{\mathrm{Bulk}}_{\mathrm{Ni}} - E^{\mathrm{Bulk}}_{\mathrm{Cr}})/A, \tag{3}$$

where $E^{*}_{\mathrm{Ni/Cr}} = E_{\mathrm{Ni/Cr}} - \sigma^{(\prime)}_{\mathrm{Ni}} A - \sigma^{(\prime)}_{\mathrm{Cr}} A$ is total energy of the Ni/Cr supercell corrected for the free surfaces of the Ni and Cr parts of the Ni/Cr supercell slab embedded in vacuum. $E^{\mathrm{Bulk}}_{\mathrm{Ni}}$, $E^{\mathrm{Bulk}}_{\mathrm{Cr}}$ correspond to the total energies of Ni and Cr in "bulk states", and $\sigma^{(\prime)}_{\mathrm{Ni}}$ and $\sigma^{(\prime)}_{\mathrm{Cr}}$ are the surface energies of the free surfaces of the Ni and Cr slabs, respectively. The supercript prime ($\prime$) indicates that surface energy calculated at strained state. All systems, including the "bulk states", are subject to the same lateral strain imposed by the underlying lattice. The above surface energies are also calculated relative to the bulk suffering the same strain as the interface,

$$\sigma^{(\prime)}_{\mathrm{X}} = (E_{\mathrm{X}} - E^{\mathrm{Bulk}}_{\mathrm{X}})/2A, \tag{4}$$

where X stands for Ni or Cr. For all the surface/interfacial energies calculations, the reference bulk energies are calculated by the incremental method. [31] For example, the reference bulk energy of Cr layer is obtained as half the energy difference between supercells containing 9-Cr(110) and 7-Cr(110) layers (similarly, one-third of the energy difference between 10-Ni(111) and 7-Ni(111) for Ni). We would like to recall that the surface energy calculated using the incremental method[31] does not strictly correspond to the exact surface energy (which is defined as the excess energy relative to the constant bulk energy). That is because the reference bulk energy itself depends on the number of layers, and thus it influences the convergence of the surface energy. Furthermore, it was shown that the surface energy of thin film exhibits oscillation with increasing number of layers due to the quantum size effect. [32–34] In the present work, however, the size of the errors associated with the above effects for the chosen number of layers is negligible comparing to the magnitude of interfacial energies. The incremental method is adopted to avoid the nearly linearly increased error in the calculated surface energy with increasing number of layers due to the computational error in the reference bulk energy. [31] Alternatively, one may treat the bulk energy as an adjustable parameter to make the surface energy oscillating around a horizontal line with respect to the number of layers, as shown in the works of Han et al. [32–34]

Combining Eqs. 2, 3, and 4, the interfacial energy can also be expressed as

$$\gamma = \sigma^{(\prime)}_{\mathrm{Ni}} + \sigma^{(\prime)}_{\mathrm{Cr}} - W, \tag{5}$$

Equation 5 presents the relationship between $W$ and $\gamma$, and expresses the fact that the interfacial energy varies essentially opposite to the work of separation. [35]

### *2.4. The averaging scheme*

Our previous study for the Fe/Ag interface has shown that a proper designed "averaging scheme" may serve as an useful method to estimate the work of separation and interfacial energy of the semicoherent /incoherent interface. [20] Based on pure DFT calculations, Benedek *et al*. [5] investigated the MgO/Cu interface using a rather large supercell (399 atoms) to take into account the lattice constant mismatch and atomic relaxation at the interface. They showed that the work of separation of real equilibrium interfaces may be reproduced as weighted averages of the work of separation of coherent interfaces calculated for translation states with high symmetry (top-site, fcc-site, bridge-site, etc.). A similar averaging scheme was also adopted by Hashibon *et al*. [29] to estimate the work of separation and interfacial energy of the incoherent Cu/Ta interface, however, without testing its transferability. However, our previous investigation in the Fe/Ag system showed that whether the averaged interfacial energy is able to reproduce the interfacial energy from direct calculations

highly depends on the response of surface energy with respect to the strains at coherent state, which, however, is not well understood yet. [20] In the present work, we will adopt this method and explore its transferability in the case of the Ni/Cr interface which has a more complex magnetic structure. In the following, we will give a brief introduction to the averaging scheme and for more details the readers are referred to Reference 20.

The basic idea of the averaging scheme is that the properties (i.e., work of separation or interfacial energy) of a semicoherent/incoherent interface may be represented by a (weighted) average over the contribution from all the atomic sites across the interface, assuming that the local contribution from each of these sites is the same as it is in the coherent interface with the same stacking sequence at the interface. Following this idea, [5, 29, 35, 36] the work of separation of a semicoherent/incoherent interface may be calculated by averaging the contribution from the individual sites,

$$W = \overline{W} + \delta W, \tag{6}$$

where

$$\overline{W} = \frac{1}{n}\sum_{i=1}^{n} W_i, \tag{7}$$

with $n$ being the number of Ni (Cr) atoms at the interface atomic layer and $W_i$ is the strain-free work of separation of site $i$, calculated for the coherent interface with the same stacking sequence as the site $i$ at the semicoherent/incoherent interface taking Cr (Ni) as the underlying lattice. $\delta W$ measures the deviation between $\overline{W}$ and the real work of separation of the semicoherent/incoherent interface $W$.

The interfacial energy of the semicoherent/incoherent interface is similarly defined by averaging over the coherent interfacial energies for interfacial Ni (or Cr) atoms sitting at different sites at the interface,

$$\gamma = \overline{\gamma} + \delta\gamma, \tag{8}$$

where

$$\overline{\gamma} = \frac{1}{n}\sum_{i=1}^{n} \gamma_i, \tag{9}$$

with $\gamma_i$ being the local interfacial energy contribution from Ni atom at site $i$ at the interface (or from Cr atom at site $i$ depending on the underlying lattice). $\delta\gamma$ measures the error between $\overline{\gamma}$ and $\gamma$. By definition, $\overline{W}$ and $\overline{\gamma}$ are related by

$$\overline{W} = \sigma_{\mathrm{Ni}}^{(\prime)} + \sigma_{\mathrm{Cr}}^{(\prime)} - \overline{\gamma}, \tag{10}$$

where $\sigma_{\mathrm{Ni}}^{(\prime)}$ and $\sigma_{\mathrm{Cr}}^{(\prime)}$ are the surface energies of Ni and Cr calculated under the same strains as the coherent interface.

## 3. Results and discussions

### *3.1. Coherent interface*

The calculated coherent work of separation maps for the interfaces taking Cr or Ni as underlying lattice are shown in Fig.2 (a) and (b), respectively. The maps describe the variation of the work of separation when shifting one part of the interface against the other. We can observe that when the interfacial atoms are stacked on top of each other (on-top stacking site), the interface has the lowest work of separation.

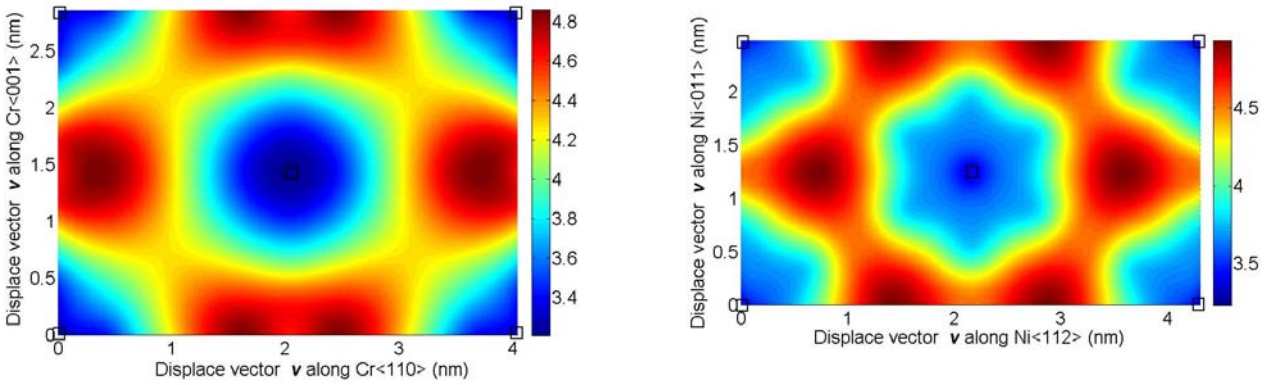


(a) (b)

Figure 2: (Color on online) The maps of the work of separation (in unit of J $m^{-2}$) of the 7-Ni(111)/7-Cr(110) coherent interfaces, (a) taking Cr as underlying lattice and (b) taking Ni as underlying lattice. The positions of the underlying interfacial atoms are marked by squares.

When the atoms across the interface maintain the fcc (ABCABC) or bcc (abababab) stacking sequences (called fcc-stacking or bcc-stacking sites), the work of separation is normally high. The calculated work of separation reflects the strength of the chemical bonding at the interface and the variation of the work of separation responding to the stacking sequence across the interface may be correlated with the interface separation. We observe that large interface separation corresponds to small work of separation, and vice versa (results of the interface separation not shown).

The typical atomic magnetic moments on each layer are shown in Fig. 3, i.e., for the coherent interface with on-top stacking sequence at the interface with Cr as underlying lattice. The bulk-like Ni atoms at the coherent strain state have similar magnetic moments as in the equilibrium (unstrained) state. All the Ni atoms keep ferromagnetic coupling, while Cr atoms keep antiferromagnetic coupling. The magnetic moments of the interface Ni atoms drop to about 0.2 $\mu_B$, while those of the interface Cr atoms increase. The magnetic moment of interface Cr is, however, smaller than that of the surface Cr atom. These observations are in agreement with previous calculations. [37]

The change in the charge density ($\Delta\rho$) upon forming the interface is calculated from

$$\Delta\rho = \rho_{\mathrm{Ni/Cr}} + \rho_{\mathrm{Ni_v}} - \rho_{\mathrm{Cr_v}}, \tag{11}$$

where $\rho_{\mathrm{Ni/Cr}}$ is the total charge density of the interface supercell, $\rho_{\mathrm{Ni_v}}$ and $\rho_{\mathrm{Cr_v}}$ are the charge densities of the separated Ni and Cr slabs, in which the atoms are frozen at their positions in the Ni/Cr interface. In Fig. 4, the charge density difference for the coherent interfaces where (a) the interface Ni atoms stacks on-top of Cr atoms (on-top stacking sequence) or (b) the interface Ni atoms sit at the hollow sites of bcc Cr(110) layer (fcc-stacking sequence) are shown. The isosurface shown in the figure corresponds to a density of 0.01 $e/\mathrm{Å}^3$. The negative density corresponds to a

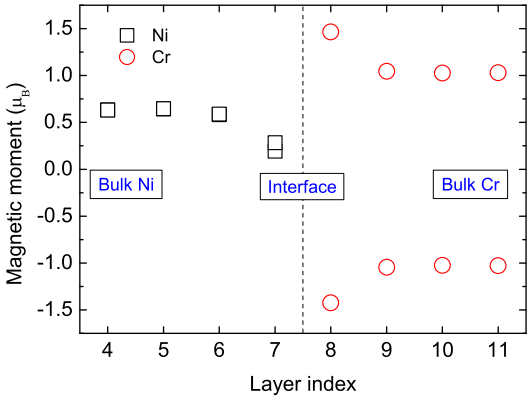


Figure 3: (Color online) The atomic magnetic moment on different layers in the 7-Ni(111)/7-Cr(110) coherent interface with on-top stacking at the interface. Each layer contains two atoms.

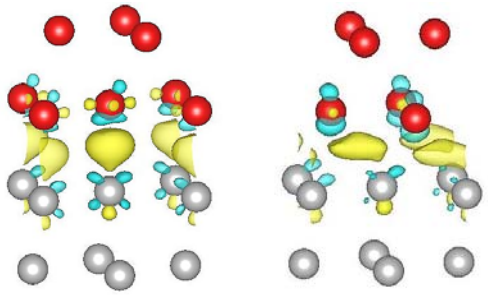

(a) (b)

Figure 4: (Color online) The charge density difference for the coherent interfaces with (a) on-top stacking sequence and (b) fcc stacking sequence, respectively. The isosurface referrers to a density of 0.01 $e/\text{Å}^3$. Positive and negative values are indicated by yellow and blue colors, respectively. Red and gray balls correspond to Ni and Cr atoms, respectively. Only the first and second layers close to the interface are shown.

deficit of electrons and the positive density to an excess of electrons. We can observe that in general only the electrons from the first-nearest interface layers contribute to bonding at the interface. Electrons deplete from the interfacial Ni and Cr atoms and accumulate at the interface between Ni and Cr layers. The isosurfaces at the interfaces for the two different stacking sequences have different shapes. One can see that the fcc-stacking sequence leads to more expanded isosurface along the interface.

The interfacial energies are calculated according to Eq. 5. Note that for calculating the coherent interfacial energy, the surface energies of the strained Ni or Cr are involved. According to Eq. 4, the surface energy for a strained lattice is defined in a way that the strain energy does not enter the surface energy. The response of surface energy with respect to the lateral strains for the Ni(111) and Cr(110) surfaces are

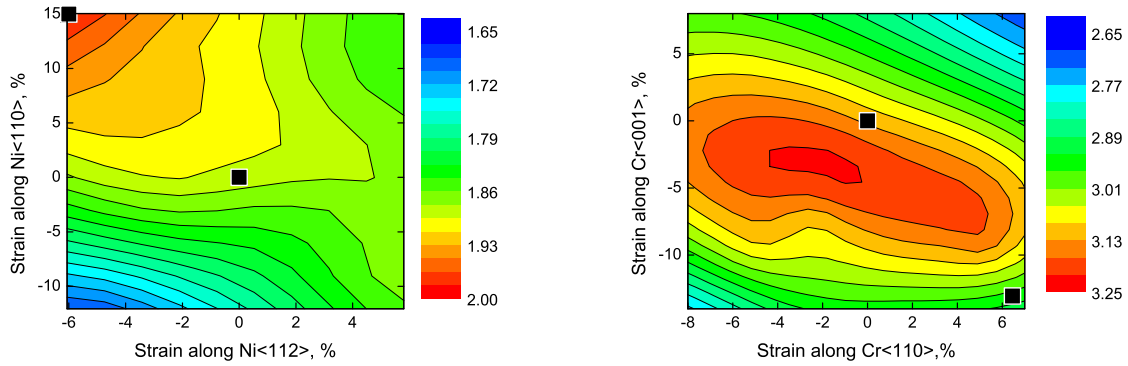


(a) (b)

Figure 5: The maps of surface energy (in unit of J $m^{-2}$) with respect to strains for (a) Ni(111) and (b) Cr(110). The surface energies for the equilibrium lattice and for the strained Ni(/Cr) lattice when taking Cr(/Ni) as underlying lattice are marked by black squares on the maps. The strains are expressed in percentage.

plotted in Fig. 5 (a) and (b), respectively. Under any lateral strain, relaxation normal to the surface is allowed. The surface energies of Ni(111) and Cr(110) calculated at equilibrium state are 1.89 J $m^{-2}$ and 3.11 J $m^{-2}$, respectively, in agreement with previous theoretical results (1.92 J $m^{-2}$ and 3.10 J $m^{-2}$, respectively[38] ). From these maps we can see that distorting Ni to match Cr coherently increases the surface energy of Ni (from 1.89 J $m^{-2}$ to 1.94 J $m^{-2}$), while distorting Cr to match Ni coherently decreases the surface energy of Cr (from 3.11 J $m^{-2}$ to 2.75 J $m^{-2}$). Therefore, according to Eq. 5 we expect that the coherent interfacial energy for case I is larger than the one for case II.

### *3.2. Semicoherent interface*

In experiments, [8, 9] the Ni-rich/Cr-rich phase interface was observed to have the $(1\bar{2}1)_{\rm fcc}$ habit plane. The $(1\bar{1}1)_{\rm fcc}$ and $(101)_{\rm bcc}$ conjugated planes of the (near) K-S OR have a one-to-one matching region for about 50 nm along the habit plane. The regions are separated by irregular distributed growth ledges. Misfit on the conjugated planes when they cross the habit plane is compensated by irregularly spaced dislocations lying in the conjugated planes. Within the scheme of the first-principles calculations, it is, unfortunately, difficult to model a realistic interface as observed in experiments. In the present work, a large supercell is employed to model an semicoherent interface and calculate the work of separation and interfacial energy. The supercell is built with $(111)_{\rm fcc}\|(110)_{\rm bcc}$, placing Ni<110>$\|$Cr<111> ($x$ direction) and Ni<112>$\|$Cr<221> ($y$ direction), which therefore keeps the near-K-S orientation relationship. Along the Ni<112> and Ni<110> directions, the equilibrium lattice parameters are 21.54 Åand 4.97 Å, respectively. Along the Cr<221> and Cr<111> directions, the equilibrium lattice parameters are 21.02 Åand 4.95 Å, respectively. The supercell is composed of 7 Cr(110) and 7 Ni(111) layers and contains 126 Cr atoms and 140 Ni atoms in total. The interface configuration is show in Fig. 6.

First, we keep Cr as the underlying lattice (case I). Then Ni lattice is distorted by -2.41% (compressed) along Ni<112> and by -0.36% (compressed) along Ni<110> directions, respectively. We preform spin polarized calculations with ferromagnetic Ni and antiferromagnetic Cr. We find the equilibrium volume of the supercell by allowing lattice relaxation along the direction normal to the interface. Atomic positions are fully relaxed until the forces on each atom are less than 0.02 ev/Å. For this interface, the work of separation and interfacial energy are 4.29 J $m^{-2}$ and 0.66 J $m^{-2}$, respectively. The surface energy ($\sigma'_{Ni}$) of Ni(111) under this strain state is calculated to be ∼1.84 J $m^{-2}$, smaller than the equilibrium value ($\sigma_{Ni}$ = 1.89 J $m^{-2}$), which agrees with surface energy map shown in Fig. 5.

When we take Ni as the underlying lattice (case II), Cr lattice is distorted by 2.46% (expanded) along the Cr<221> direction and by 0.38% (expanded) along Cr<111> direction. The work of separation and interfacial energy are 4.23 J $m^{-2}$ and 0.67 J $m^{-2}$, respectively.

Hence, for case I and case II, we get very close results, which is probably because of the relative small interface lattice misfits. Similar results for the Fe/Ag interface were also reported. [20] Wang et al. [39] calculated the work of separation of the $Al_2O_3$/Al interface and found that the variation is by less than 5% over the entire range extending from compression of Al by 4% to expansion of $Al_2O_3$ by 4%. For the Si/Cu interface, they also showed that the work of separation calculated for a fully relaxed coherent interface, where both Cu and Si lattice are highly distorted, is very close to a more accurate value calculated by a very large supercell. [40] From the above results, we may expect that the work of separation is not very sensitive to the strains, but is more affected by the atomic configurations at the interface as shown in Fig. 2.

The present calculated interfacial energies are about two times larger than the experimental value (0.30 J $m^{-2}$) reported by Hoptkins et al. [11]. One reason is that the real interface has more complex structure than the sharp interface (both composition and structure) we adopt here. The interface ledges maybe efficiently decrease the interfacial energy. [12, 13] In the experiments, the samples were held at temperature range 625-800 °C for time up to 100 hours. [11] Estimating from the Ni-Cr phase diagram [28], the measured Ni-rich phase is estimated to contain about 30-40 wt.% Cr, while the Cr-rich phase is almost pure Cr (about 98 wt.% Cr). Considering the smaller composition difference across the interface, we also expect smaller interfacial energy in practice. The other important reason may be related to magnetism. The Curie temperature of Ni is about 630 K. [41] In Ni-Cr alloys, the Curie temperature and the mean/saturate magnetic moments decreases rapidly with Cr concentration and vanishes at about 12 at.% Cr. [42] Cr impurity strongly affects

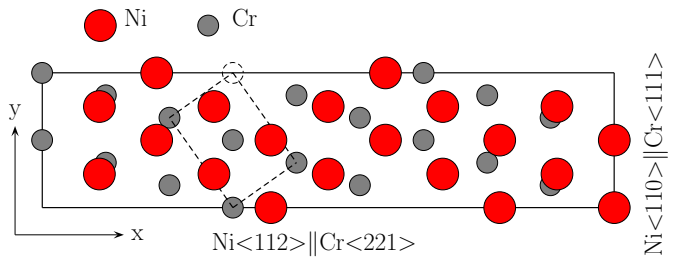


Figure 6: (Color online) Atomic configuration at the semicoherent interface.

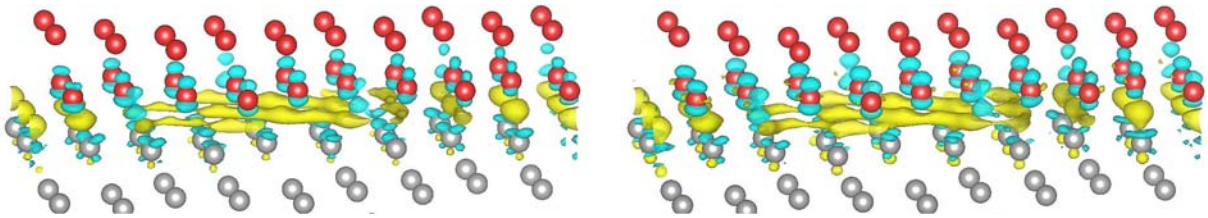

(a) (b)

Figure 7: The charge density difference for (a) magnetic and (b) non-magnetic interfaces of 7-Ni(111)/7-Cr(110), respectively. See the caption of Fig. 4.

the magnetic structure of Ni matrix. Neutron scattering experiments showed that the losses of magnetization are quite wide-spread and extend from a solute site to about 5Å. [42] The Néel temperature of Cr is 308K. Therefore, the measured eutectic phases in Reference 11 are at paramagnetic state rather than ferromagnetic state as we assume in the above calculations.

To estimate the magnetic contribution to the work of separation and interfacial energy, we perform non-spin polarized calculations with the same lattice parameters as for the polarized cases. For case I with Cr as the underlying lattice, we obtain 4.78 J $m^{-2}$ for work of separation and 0.37 J $m^{-2}$ for interfacial energy. The surface energies of Ni and Cr at nonmagnetic state is 1.92 J $m^{-2}$ and 3.24 J $m^{-2}$, respectively. The increase of the surface energy by removing magnetism is in line with previous results. [43] We can see that removing magnetism decreases the interfacial energy by ∼47%. To be more consistent, we repeat the calculations taking the equilibrium non-magnetic Cr as the underlying lattice. For non-spin polarized calculations, the equilibrium lattice constants of fcc-Ni and bcc-Cr are 3.51 Å and 2.84 Å, respectively. These values differ from the surface energies at magnetic state only by 0.28% for Ni and 1.39% for Cr. The lattice constants of the supercell with the nonmagnetic Cr as the underlying lattice are 20.89 Å along $x$ direction and 4.93 Å along $y$ direction. In this case, the mismatches between nonmagnetic Cr and nonmagnetic Ni along $x$ and $y$ directions are about 2.8% and 0.74%, respectively. The calculated work of separation and interfacial energy are 4.80 J $m^{-2}$ and 0.36 J $m^{-2}$, respectively. These results indicate that the small difference in lattice parameters between ferromagnetic and non-magnetic states does not result in sizable changes in either work of separation or interfacial energy. The surface energies under the same strain as this nonmagnetic interface are calculated to be 3.24 J $m^{-2}$ for Cr and 1.91 J $m^{-2}$ for Ni.

For case II with Ni as the underlying lattice, non-spin polarized calculations also lead to larger work of separation (4.77 J $m^{-2}$) and smaller interfacial energy (∼0.35 J $m^{-2}$). Therefore, we expect that increasing the Cr concentration in the Ni-rich phase will significantly decrease the interfacial energy, considering the fact that diminishing the composition difference across the interface is coupled with the rapid decrease in magnetization. The composition dependence of the interfacial energy of the interface between Ni-rich phase and pure Cr was studied by Chen et al. [14] using the embedded-atom method. Without considering the magnetism, they only found a very weak composition dependence of the interfacial energy, namely increasing the concentration of Cr in Ni-rich phase from 0 to 50 at.% decreases the interfacial energy from 0.216 J $m^{-2}$ to 0.200 J $m^{-2}$.

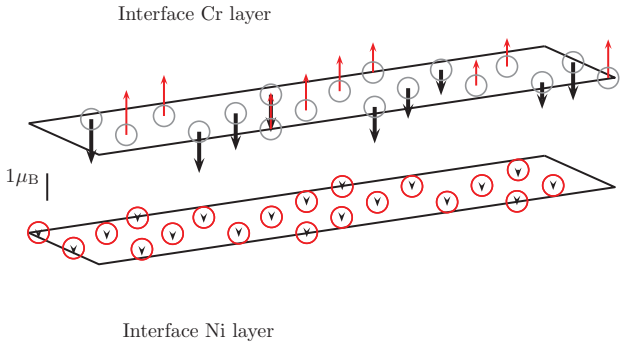


Figure 8: (Color online) Magnetic moments of the interfacial atoms.

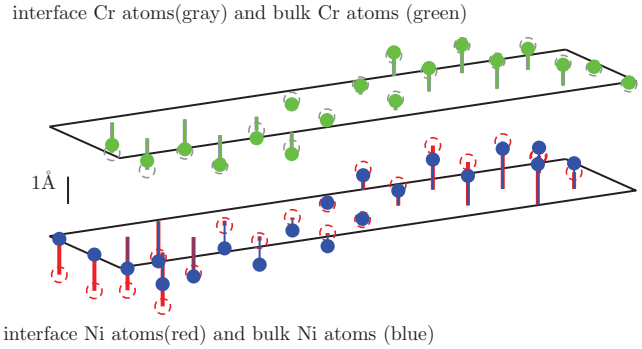


Figure 9: (Color online) Atomic displacement along the direction normal to the interface. Displacement of interfacial atoms and bulk atoms are superposed. Interfacial and bulk Cr atoms are represented by empty gray and solid green circles, respectively. Interfacial and bulk Ni atoms are represented by empty red and solid blue circles, respectively.

In Fig. 7, we show the charge density difference for the semicoherent interfaces at the magnetic (a) and nonmagnetic states (b). The local shape of the isosurface changes significantly for different atomic stacking accosts the interface, which is consistent with features shown in Fig. 4. At those sites close to the fcc-stacking sequence, the isosurfaces connect with each other and expand along the interface. While for the sites with (/close to) the on-top stacking sequence, the isosurfaces are more localized and isolated. Comparing to the magnetic interface, we can observe that at the nonmagnetic interface there are more excess electrons, which may explain the stronger chemical bonding exhibited by the larger work of separation of the nonmagnetic interface.

In Fig. 8, we plot the magnetic moments of the interfacial atoms. The interfacial Cr atoms maintain anti-ferromagnetic and have larger magnetic moments than the bulk ones (but smaller than the surface magnetic moments). The magnetic moments of the interfacial Ni atoms significantly decrease to around 0.2 $\mu_B$ due to magnetic frustration at the interface, which is in line with the observation that the magnetization of Ni decreases with increasing Cr concentration in Ni-Cr alloys. [42] The significant drop of the magnetic moment on Ni atoms is only limited to the first-nearest layer to the interface.

Table 1: Work of separation and interfacial energy of the semicoherent interface at magnetic state obtained from direct calculations and from the averaging scheme. Surface energies calculated at coherent stained state are listed. All energies are expressed in J $m^{-2}$.

| Underlying lattice | $W$ | $\gamma$ | $\overline{W}$ | $\overline{\gamma}$ | $\sigma_{\rm Ni}^{(\prime)}$ | $\sigma_{\rm Cr}^{(\prime)}$ |
|---|---|---|---|---|---|---|
| Cr lattice | 4.29 | 0.66 | 4.18 | 0.87 | 1.94 | 3.11 |
| Ni lattice | 4.23 | 0.67 | 4.41 | 0.23 | 1.89 | 2.75 |

The atomic displacement along the direction perpendicular to the interface is plotted for the 7-Ni(111)/7-Cr(110) interface in Fig. 9. Displacement vectors for the interfacial and bulk atoms are superposed and are plotted relative to the averaged atomic plane. We observe that the interface atoms have shuffled from a plane and form a buckling surface. We notice that the bulk atomic layers are also buckling because of the relative small supercell size. Increasing the size of the supercell, the buckling in the bulk planes eases in magnitude. However, the not-converged buckling in the bulk layers does not significantly affect our results of work of separation and interfacial energy. For example, calculations for the 9-Cr(110)/7-Ni(111) interface yield 4.26 J $m^{-2}$ for the work of separation, comparing to 4.29 J $m^{-2}$ for the 7-Cr(110)/7-Ni(111) interface. Even for the case that the positions of the center layers of the 7-Cr(110)/7-Ni(111) interface are fixed, we get almost the same work of separation (4.27 J $m^{-2}$). The buckling originates from the different atomic stacking at the interface, which is analogous to the cases of coherent interfaces with different stacking sequences. We place one layer of Ni on the 7 layers of Cr separated by vacuum (7-Cr(110)/Ni(111)+vacuum) and fully relax the atomic positions. We find that even in this extreme situation the interface buckling is of the similar magnitude as for the case of the 7-Cr(110)/7-Ni(111) interface. The magnitude of atomic shuffling gradually decreases from the interface to the Cr surface.

### *3.3. The averaging scheme applied to the semicoherent interfaces*

The averaging scheme described in Section II.C is applied to estimate the work of separation for case I and II based on the maps of the coherent work of separation in Fig. 2 (a) and (b). Results are listed in Table 1, together with the above results from direct supercell calculations. We get 4.18 J $m^{-2}$ and 4.41 J $m^{-2}$ for case I and case II, respectively. Comparing to the values from direct calculations, the errors are less than 5%. Similar accuracy was reached for the Fe/Ag interface. [20] However, applying the averaging scheme for the interfacial energy results in very bad agreements with the direct calculations. For case I and case II, the averaging scheme gives 0.87 J $m^{-2}$ and 0.23 J $m^{-2}$ for the interfacial energy, respectively. The large discrepancy arises from the surface energy behavior with respect to the strains as shown in Fig. 5. As already pointed out in Section III.A, the coherent interfacial energies when taking Cr as the underlying lattice are generally larger than the corresponding ones when taking Ni as the underlying lattice. This feature is reserved when applying the averaging scheme to estimate the interfacial energy for the semicoherent interfaces.

## 4. Conclusion

In the present work, we calculated the work of separation and interfacial energy for the coherent and semicoherent Ni(111)/Cr(110) interfaces by first-principles calculations. For the coherent interface, we studied the response of work of separation with respect to the stacking sequence at the interface. It is showed that the work of separation is the smallest when the interface atoms locate ontop of each other. The surface energies calculated at the same strained state as the coherent interface are involved when calculating the interfacial energy. We discussed the calculated surface energy maps for Ni(111) and Cr(110) with respect to different lateral strains. Our results indicate that the coherent interfaces formed under different strain conditions have different interfacial energies.

For the Ni(111)/Cr(110) semicoherent interfaces at magnetic state, without explicitly considering misfit dislocations, the work of separation and interfacial energy were calculated to be 4.23∼4.29 J $m^{-2}$ and 0.66∼0.67 J $m^{-2}$, respectively, depending on taking Ni or Cr as the underlying lattice. We found that magnetism has significant effect on the interfacial energy. By removing magnetism, the interfacial energy deceases to ∼0.36 J $m^{-2}$, which agrees well with the experimental value. Considering the fact that with increasing Cr content in the Ni-rich phase ($c_{Cr}\leq$12 at.%), both of Curie temperature and magnetization decrease rapidly, our results suggest that the composition dependence of the interfacial energy is strong due to the combined effects from composition and magnetism.

The averaging scheme was explored to reproduce the work of separation and interfacial energy of the semicoherent interfaces based on the results for coherent interface. We showed that the estimated work of separation by the averaging scheme differs from the values by direct calculations by only 5%. However, when applying the averaging scheme to estimate the interfacial energy, the error is large. This error is traced back to the behavior of the surface energy under strains.

## Acknowledgment

Authors acknowledge the Swedish Research Council, the European Research Council, the Swedish Foundation for International Cooperation in Research and Higher Education, the Hungarian Scientific Research Fund (research project OTKA 84078 and 109570), the Swedish Steel Producer's Association, and the Carl Tryggers Foundation for financial support. H.L. Zhang thanks to the National Science Foundation of China (No.51301126) for financial support. Q.M. Hu thanks to the MoST of China for financial support under Grant No. 2014CB644001. The National Supercomputer Centre (NSC) at Linköping University in Sweden is acknowledged for providing computational resources.

## References

[1] Kozeschnik E 2008 *Scripta Mater.* **59** 1018

[2] Shi R, Ma N and Wang Y 2012 *Acta Mater.* **60** 4172

[3] Wang Y and Li J 2010 *Acta Mater.* **58** 1212

[4] Tóth G I, Morris J R and Gránásy L 2011 *Phys. Rev. Lett.* **106** 045701

[5] Benedek R, Alavi A, Seidman D N, Yang L H, Muller D A and Woodward C 2000 *Phys. Rev. Lett.* **84** 3362

[6] Luo C P and Weatherly G C 1988 *Philo. Mag. A* **58** 445

[7] Luo C, Dahmen U and Westmacott K 1994 *Acta Metall. Mater.* **42** 1923

[8] Chen J K, Chen G and Reynolds W T 1998 *Philo. Mag. A* **78** 405

[9] Chen G, Spanos G, Masumura R and Jr W R 2005 *Acta Mater.* **53** 895

[10] Adachi Y, Hakata K and Tsuzaki K 2005 *Mater. Sci. Eng. A* **412** 252

[11] Hopkins R and Kossowsky R 1971 *Acta Metall.* **19** 203

[12] Rigsbee J and Aaronson H 1979 *Acta Metall.* **27** 351.

[13] Hall M, Aaronson H and Kinsma K 1972 *Surf. Sci.* **31** 257

[14] Chen J, Farkas D and Jr W R 1997 *Acta Mater.* **45** 4415

[15] Wang B and Urbassek H M 2013 *Phys. Rev. B* **87** 104108

[16] Yang Z and Johnson R A 1993 *Model. Simul. Mater. Sci. Eng.* **1** 707

[17] Hohenberg P and Kohn W 1964 *Phys. Rev.* **136** B864

[18] Fujii T, Nakazawa H, Kato M and Dahmen U 2000 *Acta Mater.* **48** 1033

[19] Benoit M, Langlois C, Combe N, Tang H and Casanove M J 2012 *Phys. Rev. B* **86** 075460

[20] Lu S, Hu Q M, Punkkinen M P J, Johansson B and Vitos L 2013 *Phys. Rev. B* **87** 224104

[21] Hashibon A, Schravendijk P, Elsässer C and Gumbsch P 2009 *Phil. Mag.* **89** 3413

[22] Hu S, Baskes M, Stan M and Chen L 2006 *Acta Mater.* **54** 4699

[23] Kresse G and Hafner J 1993 *Phys. Rev. B* **47** 558

[24] Kresse G and Furthmüller J 1996 *Phys. Rev. B* **54** 11169

[25] Kresse G and Joubert D 1999 *Phys. Rev. B* **59** 1758

[26] Perdew J P, Burke K and Ernzerhof M 1996 *Phys. Rev. Lett.* **77** 3865

[27] Blöchl P E 1994 *Phys. Rev. B* **50** 17953

[28] Nash P 1986 *Bull. Alloy Phase Diagr.* **7** 466

[29] Hashibon A, Elsässer C, Mishin Y and Gumbsch P 2007 *Phys. Rev. B* **76** 245434

[30] Hashibon A, Elsässer C and Rühle M 2005 *Acta Mater.* **53** 5323

[31] Boettger J C 1994 *Phys. Rev. B* **49** 16798

[32] Han Y, Evans J W and Liu D J 2008 *Surf. Sci.* **14** 2532

[33] Han Y and Liu D J 2009 *Phys. Rev. B* **80** 155404

[34] Han Y, Ünal B, Jing D, Thiel, Evans J W and Liu D J 2010 *Materials* **3** 3965

[35] Benedek R, Seidman D N and Woodward C 2002 *J. Phys.: Condensed Matter* **14** 2877

[36] Johansson S A E, Christensen M and Wahnström G 2005 *Phys. Rev. Lett.* **95** 226108

[37] Hasegawa H 1991 *Phys. Rev. B* **43** 10803

[38] Punkkinen M, Hu Q M, Kwon S, Johansson B, Kollár J and Vitos L 2011 *Philo. Mag.* **91** 3627

[39] Wang X G, Smith J R and Evans A 2002 *Phys. Rev. Lett.* **89** 286102

[40] Wang X G and Smith J R 2005 *Phys. Rev. Lett.* **95** 156102

[41] Suresh Babu V, Pavlovic A S and Seehra M S 1996 *J. Appl. Phys.* **79** 5230

[42] Besnus M J, Gottehrer Y and Munschy G 1972 *Phys. Status Solidi (b)* **49** 597

[43] Punkkinen M P J, Kwon S K, Kollár J, Johansson B and Vitos L 2011 *Phys. Rev. Lett.* **106** 057202